Is there an optimal wavelength for germicidal ultraviolet air disinfection?

Zhe Peng[1,2]*, Ben Ma[3], Daven K. Henze[4], Shelly L. Miller[4], Joost A. de Gouw[2], Jose L. Jimenez[2]*

[1] College of Environment and Climate, Guangdong−Hongkong−Macau Joint Laboratory of Collaborative Innovation for Environmental Quality, Jinan University, Guangzhou 511443, China
[2] Department of Chemistry and Cooperative Institute for Research in Environmental Sciences (CIRES), University of Colorado, Boulder, CO 80309, USA
[3] Department of Civil and Environmental Engineering, University of Nevada, Reno, NV 89557, USA
[4] Paul M. Rady Department of Mechanical Engineering, University of Colorado, Boulder, CO 80309, USA

* Corresponding authors.
Email: pengz@jnu.edu.cn (Z.P.); jose.jimenez@colorado.edu (J.L.J.)

Abstract

Germicidal UV (GUV) disinfection is effective against airborne pathogens, but it has been recently reported to increase indoor air pollution. Conventional GUV at 254 nm is applied in the upper room only due to skin/eye safety limits, while “Far UVC” (e.g. at 222 nm) is applied across the whole room due to less restrictive safety limits, enabling simpler installation and disinfection. We investigate GUV between 185 and 310 nm by modeling, in search of an optimal wavelength with both high disinfection and safety. For a specific fluence rate, GUV-induced air pollution health risks are at least ~20 times larger below 245 nm than above it. This is mainly due to O_3 production through O_2 photolysis below 245 nm, with a contribution from particulate matter formation from enhanced volatile organic compound oxidation. When normalized to a constant CDC-recommended disinfection rate of 5 equivalent air changes per hour (eACH), pollution risk below 245 nm is also at least ~20 times that above 245 nm. At very high disinfection rates such as 20 eACH, the difference between the ratios below and above 245 nm is smaller, but still a factor of ~20. Our results show a clear advantage of upper-room GUV vs. Far UVC for indoor air quality. These results appear robust despite substantial uncertainties in absolute disinfection efficiencies, which are a critical limitation for widespread GUV application. Thus, there is no optimal GUV wavelength across all important criteria (exposure limits, disinfection efficiency, indoor air quality, and logistic requirements), and these tradeoffs should be considered in different situations to maximize the overall benefit. Use of Far UVC may require simultaneous deployment of air cleaning for pollution. As new practical UV light sources at wavelengths other than 222 and 254 nm keep being developed, this study provides guidance for evaluating and selecting wavelength(s) for GUV air disinfection.

Synopsis

As 200-235 nm germicidal UV (GUV) leads to both more efficient air disinfection and more air pollution than 245-280 nm GUV does, multiple factors should be considered for maximal benefit of GUV deployment.

Key Words

Indoor air quality, germicidal ultraviolet, air disinfection, atmospheric chemical modeling, health effects

INTRODUCTION

For nearly a century, germicidal ultraviolet (GUV) disinfection has been applied for inactivation of airborne pathogens, which cause diseases after inhalation of aerosols containing them.[1–3] Although there were early attempts to widely implement GUV,[4] it has predominantly remained a specialized technique in medical contexts, mostly for tuberculosis transmission reduction.[3] The COVID-19 pandemic prompted research confirming the significance of airborne transmission for SARS-CoV-2 and other respiratory pathogens.[5,6] Consequently, there has been a surge in interest in various methods to remove pathogens from the air and/or inactivate them, including ventilation, filtration, and air disinfection,[6,7] with a particular focus on GUV.[3,8]

GUV involves lamps that emit light in the UVC range to irradiate indoor air, inactivating pathogens in airborne particles.[8] Traditionally, filtered mercury lamps have been employed for this purpose, with their most intense emission at 254 nm ("GUV254").[9] As exposure to 254 nm UV is harmful for humans, GUV254 can only be applied to the upper room or inside ducts.[10] Since the COVID-19 pandemic, there has been growing interest in shorter wavelengths, specifically "Far UVC" in the range of 200-235 nm. Its most popular implementation is based on KrCl* excimer lamps with a peak emission at 222 nm ("GUV222").[8] This interest is due to the fact that direct human exposure to GUV222 is much safer than to GUV254. The most recent recommendation from the American Conference of Governmental Industrial Hygienists (ACGIH) suggests that GUV222 is 29 times and 51 times safer for human eye and skin exposures than GUV254.[11] This allows irradiation of the occupied whole room and thus a simpler installation,[8] and the measured disinfection efficiency of GUV222 is often higher than that of GUV254 for airborne pathogens,[12,13] despite substantial uncertainties.[14–18] UV sources at other wavelengths (e.g., 270 and 282 nm) have also been reported to be used for pathogen inactivation, with disinfection efficiencies being wavelength-dependent.[12,19,20]

Recently there have been multiple reports that GUV can produce indoor air pollutants, e.g., O_3,[21–24] oxygenated volatile organic compounds (OVOC) and secondary organic aerosol (SOA),[23–25] sulfate aerosol,[26] and ultrafine particles (UFP).[25] These reports cover both GUV222 and GUV254, and include experiments (in both controlled and real-world settings) and numerical simulations. Nevertheless, there is a key difference between the indoor air pollution induced by GUV222 vs. GUV254: there is significant direct O_3 production through O_2 photolysis at 222 nm, which is not possible for GUV254, since O_2 cannot be photolyzed by UV with wavelengths longer than 245 nm.[27] O_3 can react with some common indoor volatile organic compounds (VOC), e.g., limonene, to form OVOC and SOA.[24,28] O_3 can also be photolyzed in the whole UVC range, producing OH radicals, the main atmospheric oxidant, which can oxidize a wide range of species in the air and also form UFP, OVOC, sulfate, and SOA.[24,26,29] O_3 can also react with NO_2 to form NO_3 radicals, another potent oxidant.[30] GUV lamps at other wavelengths are expected to induce similar chemistries, since many of the reactions described above will also be active. However, the amounts of secondary air pollutants formed from GUV at different wavelengths are different, since the UV absorption cross sections of the key species are strongly wavelength-dependent (Fig. 1A), leading to complex wavelength-dependent reaction rates.[27]

Ozone, particulate matter (PM, of which SOA is an important fraction), UFP, and many OVOC (e.g., formaldehyde) are known to have deleterious effects on human health.[31–34] There are well established quantitative relationships between human health risks and exposures to O_3[32] and PM,[33] enabling estimation of net premature mortality associated with exposure to both across a range of GUV configurations.

In addition to GUV222 and GUV254, devices emitting at other wavelengths for practical germicidal use have been developed recently. While disinfection efficiency and air pollutant production of all these GUV devices both depend on the wavelength, these dependencies are complex, and their tradeoff has never been systematically studied in a wavelength-dependent manner. Here we evaluate the ratio of GUV-induced secondary air pollution to disinfection efficacy over a wide range of wavelengths with high wavelength resolution, in search of an optimal wavelength(s) that can minimize safety issues (air pollution, UV exposure risk etc.) while achieving a certain disinfection goal.

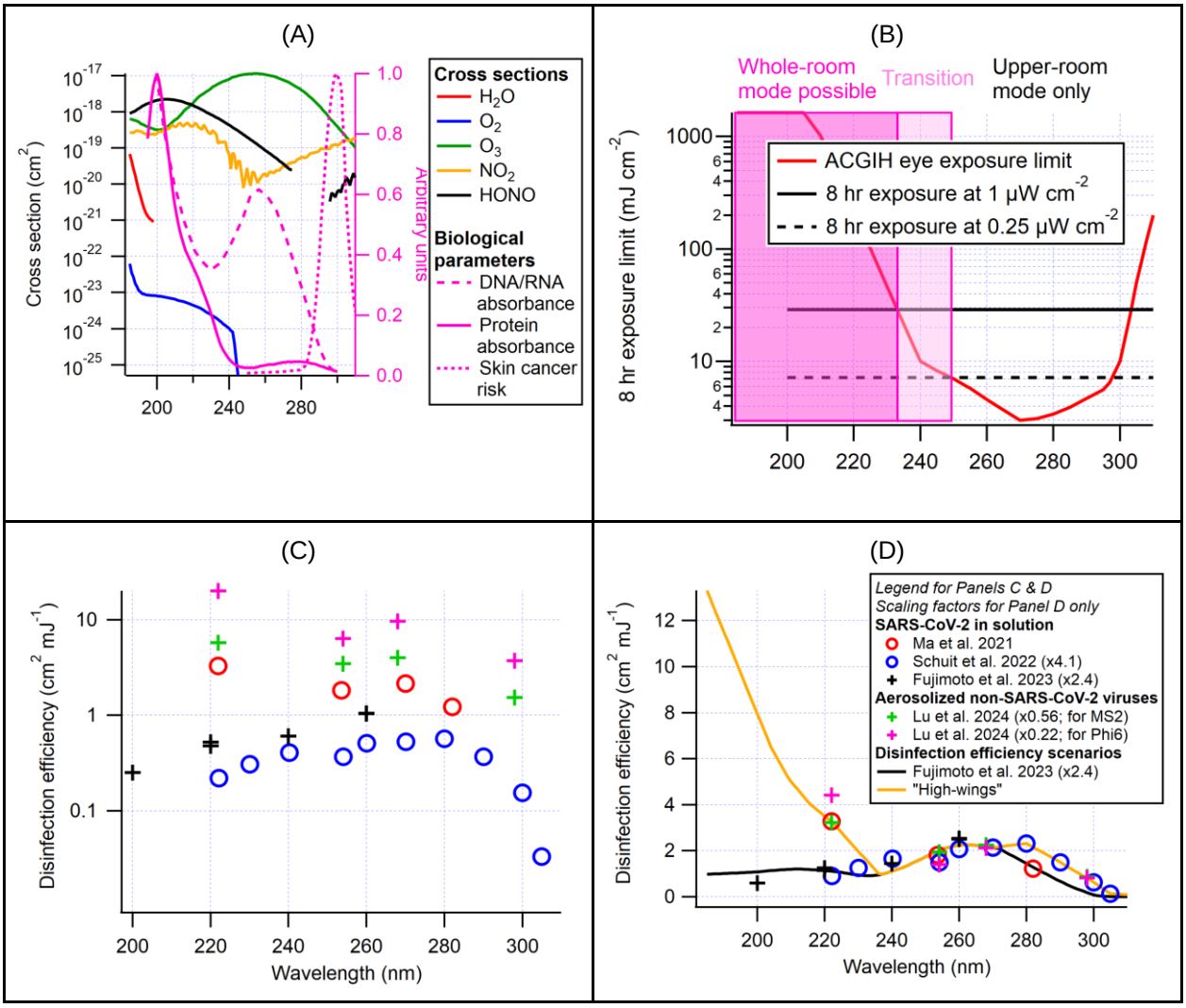

Fig. 1. Key wavelength-dependent variables between 185 and 310 nm used in this study. **(A)** Absorption cross sections of several key chemical species[35] (averaged over 1 nm intervals), relative DNA/RNA and protein absorbance, and skin cancer risk due to UV exposure.[8] **(B)** ACGIH limit of eye exposure to UV[11] and wavelength ranges for different GUV application modes; the solid and dash horizontal lines denote the 8-hour GUV exposure at 1 and 0.25 μW cm^{-2} (a typical fluence rate for GUV applications in the UVC range and a lower one for comparison), respectively. At the wavelengths in the colorless region, an 8-hour exposure at 0.25 μW cm^{-2} exceeds the ACGIH limit and/or skin cancer risk due to exposure is elevated (see Panel (A)), and thus only upper-room applications are possible. At the wavelengths in the darker pink region, 8-hour exposure at 1 μW cm^{-2} is lower than the ACGIH limit, and thus the whole-room applications can be practically possible. The lighter pink denotes the transition region, where whole-room

applications may be possible at lower fluence rates or exposure times. **(C) & (D)** Disinfection rate coefficients (k_d, in base e) from the literature (symbols) and the two scenarios used in this paper (lines) based on the fit provided by Fujimoto et al.[20] and a "high-wings" scenario (see Materials and Methods). Note that the datasets in Panel (D) are scaled by different factors to match at ~270 nm, which does not affect the relative comparison between different wavelengths.

MATERIALS AND METHODS

Indoor Air Chemical Model

The model used in this study is based on that developed in ref 23 for GUV-induced indoor air chemistry. The model in ref 23 was adapted from the chemical model of oxidation flow reactor [29] for inorganic radical chemistry under UVC irradiation. Part of the Regional Atmospheric Chemistry Mechanism[36] was added to describe organic chemistry in a simplified manner. The model has two modes, for upper- and whole-room applications, respectively. In the upper-room mode, the irradiated volume accounts for 15% of the whole room and the air exchange between the irradiated and unirradiated spaces is fast (240 and 42.4 ACH for the upper and lower parts of the room, respectively).[23] For our base case the overall room ventilation rate is kept at 1 ACH. The model runs are conducted in KinSim,[37] a chemical-kinetic solver within Igor Pro 9 (Wavemetrics, Inc., Lake Oswego, OR, USA).

Several updates to that model have been made. Several key parameters have been refined to better represent the indoor and outdoor conditions, including outdoor air composition and emission rates of indoor gases. VOC emission rates are set to values such that their steady-state concentrations in the model case with a ventilation rate of 0.4 ACH, the other settings described here, and no UV correspond to the mean values reported by Logue et al.[38] 0.4 ACH is selected as a typical ventilation rate of US residences.[39] This relatively low ventilation rate results in relatively low VOC emission rates in the base model case. The secondary pollution corresponding to these emission rates can be considered as a lower limit. We also apply penetration factors to the outdoor gas- and particle-phase species when they are transported indoors. The updates to the key parameters are detailed in Table S1.

We also update the aerosol formation and partitioning from simple literature yield-based calculations for different VOCs in ref 23 to a more detailed dynamic treatment. The framework for the dynamic aerosol formation and partitioning is based on a two-product volatility basis set (VBS), with the products being semivolatile and low-volatility species.[40] We assume the saturated vapor concentrations of the two products to be 10 and 0.0001 μg m^{-3}. Their VBS product coefficients of the oxidation of limonene, i.e., the main indoor SOA precursor, and of the second-generation oxidation of the semivolatile product to the low-volatility one were fitted to experimental results.[28] These coefficients for the other SOA precursors are estimated based on the literature yields and reported in Table S2. In addition to the partitioning between gas and particle phases, we also include gas and particle deposition onto the indoor surface, at 7.2 and 0.25 h^{-1},[41] respectively. While gas-particle partitioning is reversible, surface deposition of gas and particle products is assumed to be irreversible in the model, given the very high equivalent absorptive mass of the walls.[42]

Inorganic particle-phase species are also included in this model. Both non-volatile and volatile parts are considered, with the latter assumed to be NH_4NO_3. Inorganic aerosol concentration has no impact on the partitioning of organic species at equilibrium, but inorganic particle-phase species are assumed to form inorganic cores in aerosols in the model, which can affect the particle size and condensation and evaporation rates of organics.[43]

This model also accounts for the influence of human occupants on the indoor air composition. 10 occupants are assumed to be sitting in the room. Exhalation of CO_2 and emission of NH_3 from occupants are included, with the emission rate of 0.21 m^3 h^{-1} $person^{-1}$ and 0.4 mg h^{-1} $person^{-1}$, respectively.[44,45] For organics that occupants emit, we consider those contributing most to the total OH reactivity in the room air, i.e., isoprene and 6-methyl-5-hepten-2-one (6-MHO), whose emission rates are 260 and 19 μg h^{-1} $person^{-1}$, respectively.[46–48] Release of 6-MHO from human skin to the gas phase due to heterogeneous reactions of skin lipids and O_3 and the gas-phase reactions of 6-MHO with OH and O_3 are also taken into account.[49,50] The reactions/processes added into the model for the chemistry of isoprene and 6-MHO are listed in Table S3.

To investigate the impacts of GUV irradiation at different wavelengths, GUV is assumed to be monochromatic in individual simulations in this study. A set of 126 model runs (1 nm intervals between 185 and 310 nm) are carried out for each model case. We also assume that the UV field in the room (or the upper and lower parts of the room in the upper-room mode) is uniform. This is unrealistic for the wavelengths below 200 nm, where photoabsorption by O_2 and water vapor can cause substantial UV attenuation within a short optical pathlength.[27] But this does not affect the discussions and the conclusions of this study, as the wavelengths below 200 nm are only for illustrative purposes and not recommended for any practical GUV use.

The model requires absorption cross sections and quantum yields of all photolyzable species in the model between 185 and 310 nm. Some of those, particularly at shorter wavelengths, are unavailable in the literature and need to be estimated. We use cross sections and quantum yields from the JPL Chemical Kinetic Data Evaluation[27] and the MPI-Mainz UV/VIS Spectral Atlas of Gaseous Molecules of Atmospheric Interest[35] whenever they are available. This is the case for all photolyzable inorganic species and some photolyzable organic species. For other organic species, we adopt a strategy similar as in refs 23,51 to estimate their absorption cross sections. Unavailable cross sections at shorter wavelengths are estimated by extrapolation of data available in the literature for the wavelengths close to the unavailable ranges. Extrapolation can be done in linear or logarithmic scale, depending on the characteristics of the available data. Quantum yields are always assumed to be 1 because of the high energy of photons at the short wavelengths where estimation is required, unless the JPL Chemical Kinetic Data Evaluation[27] recommends a non-unity value.

Air Disinfection Efficiency Scenarios

GUV disinfection efficiency data are often highly uncertain and different measurements can span a very wide range. In this study, we propose two scenarios for wavelength-dependent disinfection rate coefficients (k_d) to account for the large discrepancies present in the literature studies.

The critical data for our study concerns the *relative* dependence of disinfection efficiency vs. wavelength. Absolute differences will impact the absolute amount of pollution per unit disinfection, but not the *relative* amount which is a focus of our study. To our knowledge, three studies of measurements of efficiencies of GUV inactivating SARS-CoV-2 at multiple wavelengths (covering 222 nm, 254 nm, and other wavelengths) are available.[12,19,20] Ma et al. measured a k_d (e-fold decay) of 3.27 cm^2 mJ^{-1} at 222 nm, which is in the middle of the measurements available in the literature, ranging from 1.47 to 12.4 cm^2 mJ^{-1},[14–18] while the other two studies both reported 222 nm k_d substantially lower than this range. Since ~270 nm is the main RNA/DNA absorption peak wavelength (Fig. 1A), and the absorption and disinfection near this wavelength have been relatively well studied, we use the 270 nm k_d of ref 12 as the reference and scale the values at all wavelengths reported by Schuit et al. and Fujimoto et al.[19,20] by factors of 4.1 and

2.4, respectively, so that all the three k_d at 270 nm are identical (Fig. 1D). It can be found that the relative values (peak shape) above 250 nm from these three studies are in a relatively good agreement with each other, as well as with the RNA/DNA absorbance trend at these wavelengths. The (after-scaling) k_d values for the whole wavelength range (~195-305 nm) from the fit by Fujimoto et al. are called the Fujimoto scenario, as compared to other multiwavelength measurements, the Fujimoto dataset can serve as the lower limit of the possible range of k_d after scaling (Fig. 1D). The values for <195 and >305 nm are estimated with an extrapolation based on the data at the adjacent wavelengths.

After scaling the k_d values, some diversity is observed at the lower and higher wavelengths across the literature studies. k_d above ~280 nm from Schuit et al.[19] are higher than those from Fujimoto et al.[20]. k_d at 222 nm from Ma et al.[12] is substantially higher than those at 222 nm from the other two studies. Thus we construct the "high-wings" disinfection efficiency scenario by combining the (after-scaling) k_d above 275 nm from Schuit et al., those between 235 and 275 nm from Fujimoto et al., and that at 222 nm from Ma et al. The values between 222 and 235 nm are interpolated and those below 222 nm are estimated with an extrapolation based on the RNA/DNA and protein absorbance at those wavelengths (Fig. 1A,D). The relative values between 222 and 298 nm in the "high-wings" scenario also agree well with the recent measurements of wavelength-dependent disinfection efficiencies for aerosolized viruses MS2 and Phi6[52] (Fig. 1D).

Total relative risk increase and equivalent "outdoor" concentrations of PM and O_3

Increases in either PM or O_3 can increase pollution mortality. As their changes are not proportional in different situations, it is desirable to define a single parameter that captures the overall pollution impact to simplify the analysis of this complex problem. We define a total relative risk increase (TRRI) as the combined increase in mortality risk relative to the no-UV case due to increases in various air pollutants for a given condition, i.e.,

$$TRRI = \sum_S \Delta RR_S \qquad \text{Eq. (1)}$$

where ΔRR_S is the increase in all-cause mortality risk ratio (relative risk; RR) due to pollutant S when GUV is on compared to the no-UV case. As concentration-mortality relationships, which are essential for quantifying TRRI, have been well established only for PM and O_3 to date [32,33], the TRRI in this study only includes the contributions from PM and O_3.

To estimate ΔRR_S, both the RR for pollutant S under the conditions with and without GUV need to be estimated. The latter for a typical indoor space with an outdoor concentration of S (x_o^S), denoted as $RR(x_o^S)$, can be calculated by applying the concentration-response function for pollutant S, i.e., Weichenthal et al.[33] for PM and Turner et al.[32] for O_3. Note that the concentration-response functions for common air pollutants were developed based on their outdoor concentration. RR in this study is expressed as a function of outdoor air pollutant concentration, although conceptually the health response should be a consequence of exposure to a pollutant, both outdoors and indoors, not that of outdoor concentration of that pollutant.

In the presence of GUV, the exposure to air pollutants changes compared to the no-UV case due to *indoor* concentration changes. In this case, RR cannot be calculated simply from the actual outdoor air pollutant concentration. Therefore, we define an equivalent "outdoor" concentration of pollutant S ($x_{o,eq}^S$). People spending time outdoors at this concentration and in a typical indoor space without GUV would

have the same exposure to pollutant S as they spend time outdoors at the actual concentration of S and in that indoor space with GUV. Then RR (and TRRI) can be calculated as

$$TRRI = \sum_S \left[RR\left(x_{o,eq}^S\right) - RR(x_o^S)\right] \quad \text{Eq. (2)}$$

To obtain $x_{o,eq}^S$, we consider the total exposure to S in a manner similar to Xiang et al.[53] In the absence and presence of GUV, we have

$$x_{exp,noGUV}^S = x_i^S f_i + x_o^S f_o \quad \text{Eq. (3)}$$

and

$$x_{exp,GUV}^S = (x_i^S + \Delta x_i^S) f_i + x_o^S f_o, \quad \text{Eq. (4)}$$

respectively, where $x_{exp,noGUV}^S$ and $x_{exp,noGUV}^S$ are exposure-averaged concentrations of S in the cases without and with GUV, respectively, x_i^S and Δx_i^S indoor concentration of S and its change induced by GUV, respectively, and f_i and f_o indoor and outdoor breathing rate-adjusted time fractions, respectively. With $x_{o,eq}^S$ introduced, $x_{exp,GUV}^S$ can also be written as

$$x_{exp,GUV}^S = x_{i,eq}^S f_i + x_{o,eq}^S f_o \quad \text{Eq. (5)}$$

where $x_{i,eq}^S$ is equivalent "indoor" concentration of S, which a typical indoor space without GUV would have when the outdoor concentration of S was $x_{o,eq}^S$. In this case, the indoor concentration of S is not x_i^S because there is air exchange between the air in this indoor space and the outdoor air. The indoor concentration of S varies with its outdoor concentration with an indoor-outdoor ratio, $r_{I/O}^S$. Then we have

$$\Delta x_{i,eq}^S / \Delta x_{o,eq}^S = r_{I/O}^S \quad \text{Eq. (6)}$$

where $\Delta x_{i,eq}^S = x_{i,eq}^S - x_i^S$ and $\Delta x_{o,eq}^S = x_{o,eq}^S - x_o^S$. By considering Eqs. (4-6), we obtain

$$\Delta x_{o,eq}^S = \Delta x_i^S \frac{f_i}{r_{I/O}^S f_i + f_o} \quad \text{Eq. (7)}$$

On the right side of this equation, Δx_i^S are outputs of our indoor air chemical model. In this study, we use f_i = 0.78 and f_o = 0.22.[54,55] $r_{I/O}^S$ of PM and of O_3 are assumed to be ½ and ¼, respectively.[56,57] Then $\Delta x_{o,eq}^S$ can be calculated using this equation, and TRRI obtained using Eq. (2).

RESULTS

We simulate the indoor air chemistry induced by monochromatic GUV at different wavelengths between 185 and 310 nm (1 nm interval) for both whole-room and upper-room applications (modes). We simulate a typical indoor classroom: 300 m^3 with 10 occupants, a ventilation rate of 1 air change per hour (ACH) (a value between typical US residential and commercial building ventilation rates)[39,58] with typical US

outdoor air composition, and median emission rates for indoor air pollutants, including limonene[38] (see Materials and Methods for details) as the base case for both the whole- and upper-room applications. In the upper-room mode, 15% of the room volume is irradiated by GUV. This upper-room space exchanges air with the lower part at 240 ACH (36 ACH averaged over the whole room). Sensitivity cases under different conditions are discussed below. Both modes are simulated at all wavelengths so that we can perform a comprehensive comparison in this study. In practice, use of the whole-room mode should be limited to GUV below ~235 nm, in order to comply with the eye and skin exposure limits recommended by the American Conference of Governmental Industrial Hygienists (ACGIH).[8] Whole-room applications might be allowed between 235-250 nm if the fluence rates or exposure times are lower (Fig. 1B).

Wavelengths between 185 and 200 nm are also included in the simulations to illustrate and compare the effects of the main chemical and disinfection processes at different wavelengths. Below 200 nm UV can photolyze water vapor and directly generate OH radicals in large amounts, in addition to increased O_3 production. For example, this chemistry is utilized in oxidation flow reactors to accelerate atmospheric oxidation processes.[29] In practice, UV lamps emitting in this range (e.g., unfiltered low-pressure mercury lamps) should not be used for disinfection because of their strong pollutant formation, the rapid UV decay within a short distance from the lamp that does not allow whole-room disinfection (due to strong absorption by O_2 and water vapor), and the potential health impacts of direct exposure being unclear.

We calculate ΔPM (PM concentration increase with UV relative to the concentration when there is no-UV) and ΔO_3 (O_3 increase relative to the no-UV case) vs. wavelength for both whole-room and upper-room modes. Since mortality is the largest and most serious health impact of air pollution, to summarize the air pollution impacts with a single quantity, we define a total relative risk increase (TRRI; see Materials and Methods for details) for mortality due to long-term exposure to PM and O_3 relative to the no-UV case ($TRRI = \Delta RR_{PM} + \Delta RR_{O3}$, where ΔRR_{PM} and ΔRR_{O3} are the increases in all-cause mortality risk ratios due to PM and O_3, respectively).

In the following, we first present the results for a constant fluence rate (1 μW cm^{-2}) at each wavelength, which do not involve highly uncertain wavelength-dependent disinfection efficiencies. Then, we show the results for two specific disinfection rates (5 and 30 equivalent air changes per hour (eACH)) across different wavelengths, which do involve uncertain and wavelength- and pathogen-dependent disinfection efficiencies.

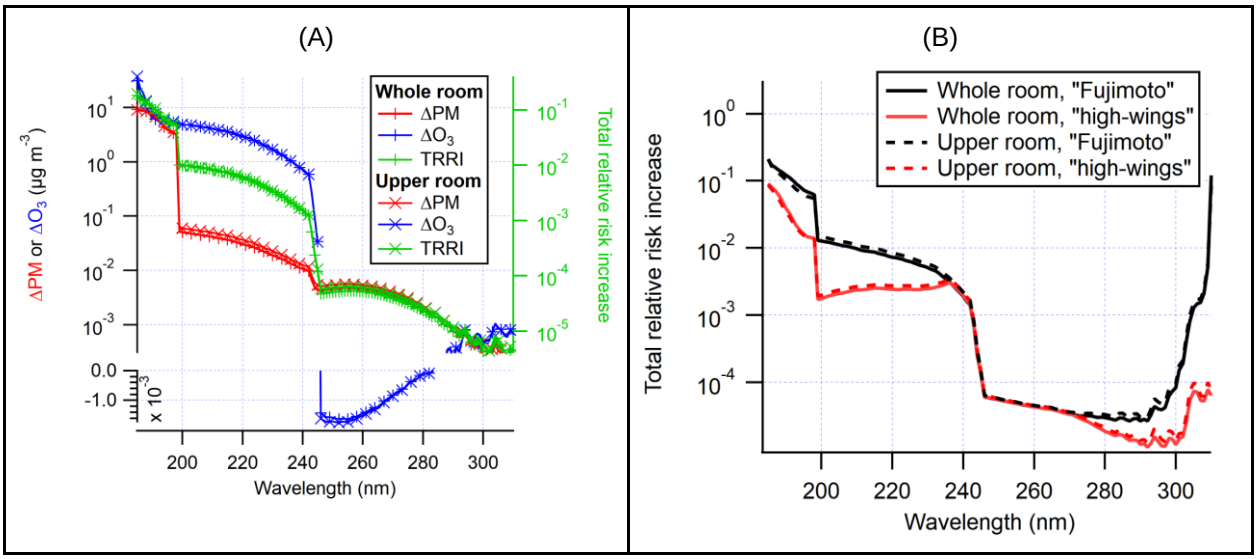

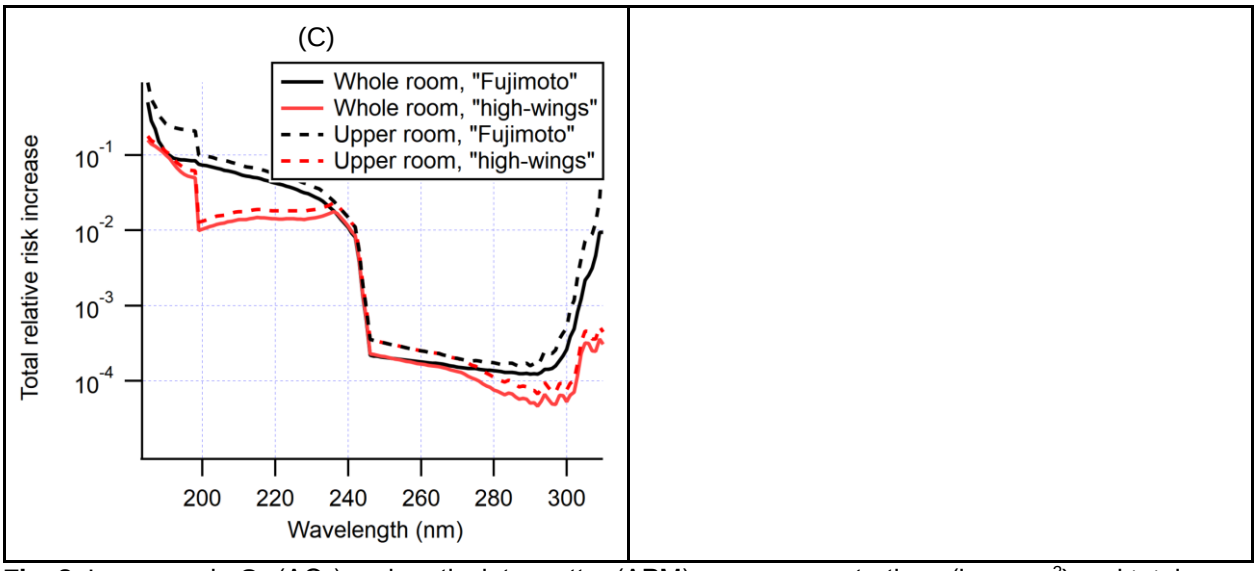

Fig. 2. Increases in O_3 (ΔO_3) and particulate matter (ΔPM) mass concentrations (in μg m^{-3}) and total relative risk increase (TRRI) relative to the no-UV case. **(A)** For a fluence rate of 1 μW cm^{-2} in both whole- and upper-room modes. Note that ΔPM and ΔO_3 are plotted along the left axis and TRRI along the right one, and that the left axis is divided into the positive and negative parts, which are in log and linear scales, respectively. **(B)** For an effective whole-room disinfection rate of 5 equivalent air changes per hour (eACH), as recommended by the CDC for COVID-19.[59] **(C)** For an effective whole-room disinfection rate of 20 eACH, comparable to CDC guidelines for upper-room GUV for tuberculosis.[60]

Constant Fluence Rate at each Wavelength

Fig. 2A shows TRRI vs. wavelength at an average fluence rate of 1 μW cm^{-2} (effective fluence rate averaged over the whole room for either mode). Mortality risk generally increases as the GUV wavelength decreases towards 185 nm. Two large jumps in TRRI occur at ~244 and ~199 nm. These correspond to large increases in ΔO_3 and in ΔPM, respectively.

Above 245 nm, O_3 cannot be directly produced through O_2 photolysis by GUV. GUV photolyzes O_3 and produces OH in a similar way as in the troposphere, i.e., via production of $O(^1D)$, which then reacts with water vapor to form OH.[27,29] As a result, ΔO_3 is negative at most wavelengths >245 nm. It becomes slightly positive only above ~290 nm, where i) O_3 photolysis is much weaker due to O_3 absorption cross section being >1 order of magnitude lower than its peak value at 254 nm, and ii) O_3 production in the same way as in the troposphere (i.e., via NO_2 photolysis, which produces $O(^3P)$ that recombines with O_2 and forms O_3) is much stronger due to the NO_2 absorption cross section being ~1 order of magnitude higher than at ~250 nm. At >245 nm, TRRI is dominated by ΔPM, almost all of which results from VOC oxidation by OH (Fig. 2A).

Below 242 nm TRRI (>~0.0013) is at least 20 times larger than at >245 nm (<~6×10^{-5}), mostly due to ΔO_3 resulting from O_2 photolysis (Fig. 2A). Although the contribution of ΔPM to TRRI is smaller compared to ΔO_3 for our base case, ΔPM in this wavelength range is substantially larger than above 245 nm. A much higher O_3 concentration at 200-242 nm promotes terpene ozonolysis and leads to most of the increase in ΔPM, consistent with Jenks et al.[28] The OH increase relative to the no-UV case in this wavelength range is of the order of 10^3 molecules cm^{-3}, and thus cannot lead to a substantially higher ΔPM than above 245 nm. TRRI monotonically increases with decreasing wavelength, because of the same trend on the (1 nm-averaged) cross section of O_2 absorption (Fig. 1A), which leads to direct O_3 production.

Below 198 nm, water vapor can be photolyzed, leading to a strong direct production of OH. Consequently, compared to 200-242 nm, OH concentration increases at least by a factor of 15. This high OH rapidly oxidizes VOCs and causes a large increase in ΔPM (and hence TRRI) by about an order of magnitude (Fig. 2A). On the other hand, O_2 absorption and ΔO_3 do not have a large increase around 199 nm, and thus do not contribute to this drastic increase in TRRI.

Note that the results of both whole- and upper-room simulations at 1 μW cm^{-2} are reported in Fig. 2A, and they are almost identical. This is due to the air exchange between the irradiated and unirradiated spaces in the upper-room mode being faster than the other production and loss processes of O_3 and PM at this fluence rate. This indicates that at 1 μW cm^{-2}, if both whole- and upper-room modes use UV light at the same wavelength (e.g., both at 222 nm), they lead to almost the same disinfection and air pollution.

Constant Disinfection Rate

We also examine mortality risk at specific disinfection rates. Two effective disinfection rates for the whole room (not only for the irradiated space, in the upper room case), i.e., 5 and 20 eACH, are investigated. The former is the value recommended by the US Centers for Disease Control and Prevention (CDC) and close to that from the World Health Organization recommendation (6 eACH) for COVID-19.[59,61] The value of 20 eACH is chosen because the mid-value of the upper-room GUV254 fluence rate range (30-50 μW cm^{-2}) recommended by the CDC for tuberculosis[60] leads to a disinfection rate close to 20 eACH in our model. The fluence rates needed to achieve these disinfection rates are different at each wavelength (Fig. S1), as they are inversely proportional to the (pathogen-specific) disinfection rate coefficients (k_d) at each wavelength. Measurements of k_d have large absolute uncertainties (1-2 orders of magnitude, Fig. 1C), but mostly consistent trends vs. wavelength (within factors of 2-3; Fig. 1D). To investigate the disinfection vs. pollution tradeoff vs. wavelength, while accounting for the differences in relative wavelength trends in the literature, we investigate two disinfection efficiency vs. wavelength scenarios (Fujimoto and "high-wings"; Fig. 1D; see Materials and Methods for details). The Fujimoto scenario is based on Fujimoto et al.;[20] the "high-wings" scenario has higher disinfection efficiencies at <235 nm and >270 nm (higher "wings" in the disinfection efficiency curve).

At 5 eACH of disinfection, the TRRI of the upper- and whole-room modes are still very close (Fig. 2B). For the Fujimoto disinfection efficiency scenario, TRRI at 5 eACH is not substantially different from that at 1 μW cm^{-2} in the wavelength range of interest of this study, except for those >290 nm. This similarity is because i) the relative variation in the disinfection efficiency coefficient (k_d; in base e, same hereafter) of this scenario with wavelength is relatively small (within a factor of 2 between 185 and 290 nm; Fig. 1D), and ii) a fluence rate of 1 μW cm^{-2} and a k_d around 1.5 cm^2 mJ^{-1} (a ballpark value for this estimate) at a ventilation rate of 1 ACH result in a disinfection rate of 5.4 eACH. The drastic increase of TRRI at 5 eACH above 290 nm corresponds to the fast decrease of the disinfection efficiency as the wavelength increases from 290 to 310 nm. When k_d is low at these wavelengths, the fluence rate needed for 5 eACH is high, which causes more secondary air pollution. Large differences between the two k_d scenarios results in high uncertainty in TRRI in this region.

For the "high-wings" disinfection efficiency scenario, TRRI at 5 eACH below 235 nm or above 275 nm is lower than that for the Fujimoto scenario (Fig. 2B). This difference is due to the higher k_d for the "high-wings" scenario at these wavelengths. TRRI at 5 eACH does not monotonically increase with decreasing wavelength between 200 and 235 nm, unlike the Fujimoto scenario (Fig. 2B), but rather stays about constant. This is due to the stronger increase of k_d in the "high-wings" scenario in this wavelength range, which allows reduced fluence rate that offsets the increased air pollution (if fluence rate is constant)

shown in Fig. 2A. TRRI at 5 eACH in the “high-wings” scenario below 235 nm is still >20 times larger than that above 250 nm, mainly due to the strong direct O_3 production by O_2 photolysis at shorter wavelengths as discussed above.

The results for 20 eACH show a significant (about 50%, Fig. 2C) difference between the upper-room and whole-room setups. When the disinfection rate is higher, the fluence rate in the irradiated space for the upper-room mode is also higher. As a result, the viable airborne pathogen (SARS-CoV-2) gradient between the unirradiated and irradiated spaces becomes more pronounced, and the disinfection rate for the whole room is limited by the transport of viable SARS-CoV-2 from the unirradiated space to the irradiated space through air exchange between these two zones. A disinfection rate of 20 eACH averaged over the whole room in the upper-room mode requires a high fluence rate that may result in the SARS-CoV-2 concentration in the upper room significantly lower than that in the lower room, depending on the airflow patterns in the room, assuming the lamps are installed in the ceiling.[23] This reduces the efficacy of the upper-room GUV and in turn requires a higher effective fluence rate (averaged over the whole room) than in a whole-room setup. According to our additional simulations at different disinfection rates (1-30 eACH; Fig. S2), this discrepancy between the two modes for a specific disinfection rate starts becoming significant at a disinfection rate ~10 eACH and increases drastically as the disinfection rate approaches the limit due to in-room air exchange, i.e., 36 eACH (for the volume of the whole room) in our simulations.

Impact of Variations in Indoor Conditions

We also investigate how the results change over large ranges of ventilation rates of 0.1-30 ACH, and of indoor VOC emission rates (relative to the base case) of 0.1-10. This sensitivity study is performed only for the “high-wings” disinfection efficiency scenario, where the TRRI at “wings” wavelengths (i.e., <235 nm and > 275 nm) is lower than in the Fujimoto scenario. Since the results above indicate that there are mainly two distinct wavelength regions (for whole- and upper-room GUV, respectively), we explore the ratio of TRRI between 222 (in the whole-room mode) and 254 nm (in the upper-room mode), the most representative wavelengths of each region, at disinfection rates of 5 and 20 eACH (Fig. 3). Even so, except for the strongest (weakest) ventilation and the weakest (strongest) indoor emissions explored, the 222 nm-to-254 nm TRRI ratio is >1 and, under most conditions, >10 (Fig. 3A,B). Moreover, the conditions with TRRI ratio <1 correspond to TRRI ratio <0, due to negative TRRI (less air pollution compared to the no-UV case) for GUV254 under these conditions. Note that the higher TRRI ratios at low ventilation rates and/or high indoor VOC emissions are no longer directly due to O_3 formed through O_2 photolysis, but mainly due to PM formed through VOC ozonolysis, as the high TRRI at 222 nm under these conditions are mostly contributed by PM (Fig. 3C). The drastic decrease of the contribution of O_3 to TRRI with decreasing ventilation rate below 0.9 ACH is associated with the equivalent “outdoor” O_3 (in terms of exposure mortality; as calculated in the way described in Materials and Methods) decreasing below the threshold in Turner et al.[32] (Fig. S3), below which no mortality risk increase due to O_3 was reported by Turner et al. Note that this lack of reported mortality risk increase in their O_3 concentration-mortality relationship resulted from scarcity of low ambient O_3 concentrations. Even at low equivalent “outdoor” O_3 concentrations, low levels of one of the two main contributors, indoor O_3, may be related to strong O_3 loss[62] and high levels of O_3 reaction products. The latter is associated with negative health effects,[63] although, to our knowledge, a quantitative concentration-mortality relationship that can be used in this study has not been developed.

(A) 5 eACH	(B) 20 e ACH

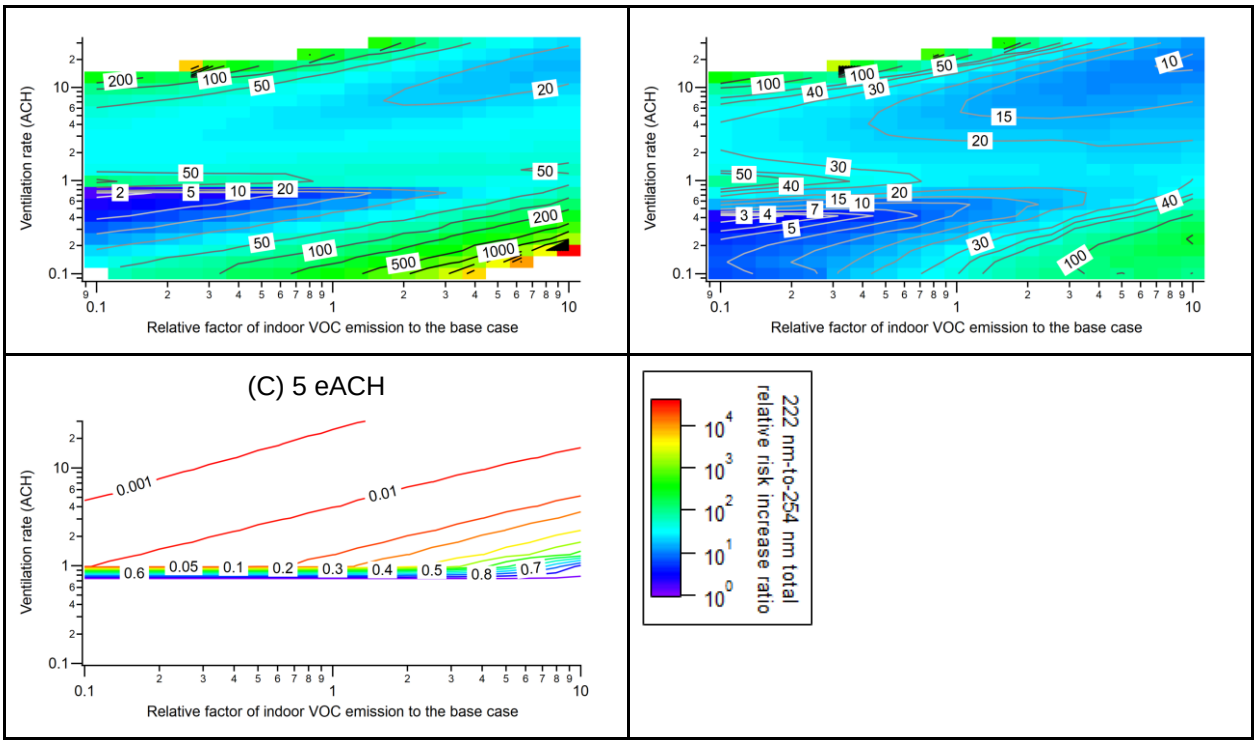

Fig. 3. Sensitivity study exploring the impacts of ventilation rate and indoor VOC emission rate for the "high-wings" disinfection efficiency scenario. **(A)** Image and contour plots of whole-room 222 nm to upper-room 254 nm total relative risk increase (TRRI) ratio at a disinfection rate of 5 eACH. **(B)** Same format for a 20 eACH disinfection rate. **(C)** Contour plot of the fractional contribution of PM to TRRI at 5 eACH. The color scale legend is for Panels (A) and (B).

DISCUSSION

In practice, GUV at 200-235 nm and that at >245 nm are almost only used for the whole-room and upper-room applications, respectively. As discussed above, wavelengths below 200 nm are of little practical interest. Because of low disinfection efficiency and high cancer risk (Fig. 1A), wavelengths above 280 nm are also not practically useful. In the following, we thus only compare 200-235 nm (shorter) and 245-280 nm (longer).

It can be concluded with high confidence that longer-wavelength (245-280 nm) upper-room GUV produces substantially less secondary indoor air pollution per unit disinfection than shorter-wavelength (200-235 nm) in whole-room applications (Fig. 2). We first discuss the uncertainties in the results, and then their implications.

Uncertainties in Disinfection Rates

The absolute values of k_d are a major source of uncertainty of the absolute pollution mortality-to-disinfection ratio, but much less so for the relative trend of that ratio with wavelength. For instance, the absolute values of k_d for SARS-CoV-2 at 222 nm reported in different studies range about two orders-of-magnitude.[14–18] If the real k_d at 222 nm is close to the high end of the range of the literature measurements (~12 cm^{-2} mJ),[16] the fluence rate needed to achieve a specific disinfection rate is about ¼

of that for the "high-wings" scenario, and the corresponding TRRI is also about ¼ of that scenario. Conversely, if the real k_d at 222 nm is close to the lower values reported in the literature, the corresponding TRRI would be an order-of-magnitude larger.

Literature k_d values for the same pathogen are generally higher in aerosols than in aqueous solutions.[64,65] The relative trend of k_d across wavelengths reported in Ma et al.[12] is consistent with RNA/DNA absorption for >245 nm and with the measurements and the explanation (higher contribution from protein and lipid damage) by Lu et al. (Fig. 1A,D).[64,66] These authors recently reported aerosol-based multiwavelength k_d measurements for other viruses than SARS-CoV-2 (MS2 and Phi6; Fig. 1C,D),[52] whose relative wavelength trend agrees well with Ma et al.,[12] but is different from other literature results.[19,20] These comparisons across wavelengths show that the relative dependence of k_d on wavelength (see Materials and Methods for detail) is within a factor of ~3 for wavelengths near 222 nm and within a factor of 2 for >245 nm for all the studies that have reported multiwavelength measurements for SARS-CoV-2 in solution and other viruses in aerosols (Fig. 1D).[12,19,20,52] This results in limited uncertainty on our conclusions about the relative trend. As the range that (after-scaling) k_d reported in the literature span is largely captured by the Fujimoto and "high-wings" scenarios, the uncertainty about the relative trend is unlikely to be substantially larger than the difference between the results of these two scenarios.

The extrapolation of k_d below 222 nm in the "high-wings" scenario could be too optimistic, as k_d is estimated to increase as fast as the protein or RNA/DNA absorption efficiencies, without accounting for aerosol shielding effects.[67] Thus the pollution per unit disinfection below 222 nm for this scenario could be a lower limit. Nevertheless, the possible underestimation of the pollution per unit disinfection below 222 nm only reinforces our conclusion that this pollution at shorter wavelengths is higher than at longer wavelengths.

Uncertainties in Pollutant Formation

There are also uncertainties associated with the chemistry model. The root cause of higher TRRI below 235 nm is O_3 produced from O_2 photolysis. This is a simple photochemical process whose kinetic parameters were well quantified decades ago.[68,69] The O_3 production rate through this pathway is governed by the O_2 absorption cross section, whose relative uncertainty is ~20%.[35] The estimation of the cross sections and quantum yields of organic species whose measurements are unavailable in the literature (see Materials and Methods for detail) may also introduce uncertainty into the model. We quantify the potential impact of this treatment for organic photolysis in the UVC range with a sensitivity case where all organic photolysis processes are removed. The relative change in ΔPM of the sensitivity case is up to ~15% below 290 nm, and within a factor of 2 between 290 and 310 nm (Fig. S4). The relative change in ΔO_3 is negligible below 245 nm but larger above this wavelength. Nevertheless, the contribution of ΔPM to TRRI between 200 and 245 nm is minor. And ΔO_3 between 245 and 290 nm is negative, of which the amplification cancels the contribution of ΔPM to TRRI in this wavelength range (Fig. 2). These lead to the very small relative change in TRRI between 200 and 290 nm. At longer wavelengths, as discussed above, practical interest of GUV is low, and the relative change in TRRI is still within a factor of ~2.

Despite the uncertainties in the k_d and the chemistry model, the difference in TRRI is so large (>1 order of magnitude) that the conclusion that longer-wavelength (245-280 nm) GUV produces much less air pollution than shorter-wavelength (<235 nm) GUV for a specific disinfection rate is robust.

Implications for the net health benefit of GUV device deployment

As ~85% of the air that people inhale is indoors[54] and typical indoor-to-outdoor O_3 ratios are ~25% in the US,[57] indoor O_3 accounts for about half of O_3 exposure of the US population. As discussed by Xiang et al.,[53] indoor O_3 exposure is a main contributor to the observed correlation between outdoor O_3 concentration and mortality. Here, based on key results of this study and some simple estimations, we consider if the mortality due to GUV-induced indoor air pollution can be significant compared to the number of lives that GUV air disinfection can save from airborne diseases.

At a fluence rate of 1 μW cm^{-2} (corresponding to a disinfection rate of several eACH for SARS-CoV-2, depending on k_d), ΔO_3 between 200 and 235 nm ranges from ~4.9 to ~1.2 μg m^{-3} (~2.5-0.6 ppb), with that at 222 nm being 2.7 μg m^{-3} (1.4 ppb). Considering the about-half contribution of indoor O_3 to O_3 exposure, we estimate such an indoor ΔO_3 of 2.7 μg m^{-3} to be equivalent to an outdoor O_3 increase of 4-5 ppb, to be used in the concentration-response relationships that have been developed only with outdoor data. This may lead to a ~0.9% increase in all-cause mortality (if O_3 increases PM as discussed above, the mortality increase could be even higher), while ~2.4% of the deaths in the US in 2023 were related to COVID-19.[70,71] For simplicity, mortalities due to both other airborne diseases (e.g., influenza and tuberculosis) and exposure to other secondary indoor air pollutants (e.g., OVOCs) are ignored here as they are expected to be smaller.[32,72] As GUV usually reduces airborne disease transmission and increases air pollution exposure of indoor space occupants at the same time, a long-term use of short-wavelength (200-235 nm) GUV devices without air pollution mitigation measures would be likely to both save lives from COVID-19 and other airborne diseases and increase mortality due to GUV-induced O_3 pollution. If GUV device installations are still too low to significantly change the dynamics of an airborne epidemic, the numbers of lives it saves and the deaths caused by its air pollution could be of the same order of magnitude. When the highest values of k_d at 222 nm reported in the literature are considered (~x4 higher than the "high-wings" value),[16] mortality due to air pollution would be an order-of-magnitude lower than lives saved from airborne diseases by GUV disinfection. GUV-induced air pollution would be a smaller but still significant concern. On the other hand, if the real k_d at 222 nm is close to the lower end of the range of the literature measurements, 222 nm GUV application might bring little net health benefit due to air pollution.

As a consequence, the traditional upper-room longer-wavelength (245-280 nm) GUV application is still of high interest, particularly for long-term use (when community transmission of airborne disease(s) of interest is sustained) at moderate fluence rates (e.g. 5 eACH), as it results in much lower GUV-induced secondary indoor air pollution and thus the related mortality by about an order of magnitude or more.

Is there an optimal GUV wavelength?

In summary, across the wavelengths explored in this study (185-310 nm), there is not an optimal wavelength that is the best in terms of disinfection efficiency, ease of practical use, secondary air pollution, and exposure safety. There are wavelength ranges obviously worse than others, i.e., 185-200 nm (due to very high secondary air pollution and nearly impossible practical functioning in real indoor settings) and 280-310 nm (due to high cancer risk and low k_d). Whole room 200-235 nm and upper-room 245-280 nm represent two regimes of operation with clear tradeoffs. In terms of air pollution per unit disinfection, longer-wavelength GUV has a clear advantage over its shorter-wavelength counterpart. Nevertheless, this advantage does not negate the less logistic requirement, ability to reduce close-range transmission, and the potentially higher k_d of shorter-wavelength GUV, and hence the highest possible disinfection rate in its whole-room application, all of which can be critically helpful for a fast response to an emerging airborne disease and suppression of an airborne epidemic. Shorter wavelength long-term applications may necessitate the integrated use of pollution scrubbers (e.g. O_3 removal catalysts and PM filters).

Current upper-room installations use mostly 254 nm, partially due to low cost of the lamps.[8] There are longer wavelengths with slightly better ratios of GUV-induced indoor air pollution per disinfection (Fig. 2). At a specific disinfection rate, GUV near 280 nm, where GUV exposure cancer risk is still relatively low (Fig. 1A), can reduce TRRI to about half compared to that at 254 nm. However, the uncertainties in disinfection rates and higher cost of operating at other wavelengths result in limited incentives to operate upper-room systems away from 254 nm. Increasing the upper room air exchange rate (e.g., with a fan) can be a way to improve the performance of upper-room GUV (in terms of air pollution per unit disinfection) when the disinfection rate needed is high.[23,60] A strong air exchange (achieved through mixing as recommended by CDC tuberculosis guidelines)[60] between the lower and upper room can limit the penalty of airborne pathogen depletion in the upper room at a high GUV fluence rate, thus lowering the fluence rate needed and reducing associated air pollution. Air pollution mitigation, such as ozone destruction and PM filtering, can be performed for both whole- and upper-room GUV, albeit at additional cost, to maximize the overall health benefit of GUV applications.

The future of whole-room shorter-wavelength GUV depends partially on more accurate determinations of k_d in the real world. If real k_d are at the lower end of the literature, its use may be limited to periods or locations with high mortality risk from airborne diseases, such as health care settings where infectious disease and/or immunocompromised patients are present, or high occupancy settings with unsuspected infectious individuals like jails and prisons. If real k_d are at the higher end of literature, wide-scale deployment with small pollution scrubbers may be attractive.

Acknowledgements: This study was supported by Balvi Filantropic Fund, the Sloan Foundation Indoor Chemistry Program, and the CIRES Innovative Research Program. We thank Charles Weschler, Julia Lee-Taylor, and Carl Bengtsson for their valuable discussions.

Author contributions: Z.P. and J.L.J. conceived this study. Z.P. designed the study, developed the model, conducted the simulations, and led the analysis of the results and the preparation of the manuscript. B.M, D.K.H., S.L.M., J.A.d.G., and J.L.J. contributed to the analysis of the results and the preparation of the manuscript.

Data and materials availability: All data needed to evaluate the conclusions in the paper are present in the paper and/or the Supporting Information. The source code of KinSim is publicly available at http://tinyurl.com/KinSim-Download. The results for this study can be downloaded from https://cires1.colorado.edu/jimenez/group_pubs.html.

References

(1) Wells, W. F.; Wells, M. W.; Wilder, T. S. The Environmental Control of Epidemic Contagion: I. An Epidemiologic Study of Radiant Disinfection of Air in Day Schools. *Am. J. Epidemiol.* **1942**, *35* (1), 97–121.
(2) Riley, R. L.; Mills, C. C.; O'grady, F.; Sultan, L. U.; Wittstadt, F.; Shivpuri, D. N. Infectiousness of Air from a Tuberculosis Ward. Ultraviolet Irradiation of Infected Air: Comparative Infectiousness of Different Patients. *Am. Rev. Respir. Dis.* **1962**, *85*, 511–525.
(3) Nardell, E. A. Air Disinfection for Airborne Infection Control with a Focus on COVID-19: Why Germicidal UV Is Essential. *Photochem. Photobiol.* **2021**, *97* (3), 493–497.
(4) Jimenez, J. L.; Marr, L. C.; Randall, K.; Ewing, E. T.; Tufekci, Z.; Greenhalgh, T.; Tellier, R.; Tang, J.

W.; Li, Y.; Morawska, L.; Mesiano-Crookston, J.; Fisman, D.; Hegarty, O.; Dancer, S. J.; Bluyssen, P. M.; Buonanno, G.; Loomans, M. G. L. C.; Bahnfleth, W. P.; Yao, M.; Sekhar, C.; Wargocki, P.; Melikov, A. K.; Prather, K. A. What Were the Historical Reasons for the Resistance to Recognizing Airborne Transmission during the COVID-19 Pandemic? *Indoor Air* **2022**, *32* (8), e13070.

(5) Greenhalgh, T.; Jimenez, J. L.; Prather, K. A.; Tufekci, Z.; Fisman, D.; Schooley, R. Ten Scientific Reasons in Support of Airborne Transmission of SARS-CoV-2. *Lancet* **2021**. https://doi.org/10.1016/S0140-6736(21)00869-2.

(6) Morawska, L.; Allen, J.; Bahnfleth, W.; Bluyssen, P. M.; Boerstra, A.; Buonanno, G.; Cao, J.; Dancer, S. J.; Floto, A.; Franchimon, F.; Greenhalgh, T.; Haworth, C.; Hogeling, J.; Isaxon, C.; Jimenez, J. L.; Kurnitski, J.; Li, Y.; Loomans, M.; Marks, G.; Marr, L. C.; Mazzarella, L.; Melikov, A. K.; Miller, S.; Milton, D. K.; Nazaroff, W.; Nielsen, P. V.; Noakes, C.; Peccia, J.; Prather, K.; Querol, X.; Sekhar, C.; Seppänen, O.; Tanabe, S.-I.; Tang, J. W.; Tellier, R.; Tham, K. W.; Wargocki, P.; Wierzbicka, A.; Yao, M. A Paradigm Shift to Combat Indoor Respiratory Infection. *Science* **2021**, *372* (6543), 689–691.

(7) Morawska, L.; Tang, J. W.; Bahnfleth, W.; Bluyssen, P. M.; Boerstra, A.; Buonanno, G.; Cao, J.; Dancer, S.; Floto, A.; Franchimon, F.; Haworth, C.; Hogeling, J.; Isaxon, C.; Jimenez, J. L.; Kurnitski, J.; Li, Y.; Loomans, M.; Marks, G.; Marr, L. C.; Mazzarella, L.; Melikov, A. K.; Miller, S.; Milton, D. K.; Nazaroff, W.; Nielsen, P. V.; Noakes, C.; Peccia, J.; Querol, X.; Sekhar, C.; Seppänen, O.; Tanabe, S.-I.; Tellier, R.; Tham, K. W.; Wargocki, P.; Wierzbicka, A.; Yao, M. How Can Airborne Transmission of COVID-19 Indoors Be Minimised? *Environ. Int.* **2020**, *142*, 105832.

(8) Blatchley, E. R., III; Brenner, D. J.; Claus, H.; Cowan, T. E.; Linden, K. G.; Liu, Y.; Mao, T.; Park, S.-J.; Piper, P. J.; Simons, R. M.; Sliney, D. H. Far UV-C Radiation: An Emerging Tool for Pandemic Control. *Crit. Rev. Environ. Sci. Technol.* **2023**, *53* (6), 733–753.

(9) Riley, R. L.; Nardell, E. A. Clearing the Air: The Theory and Application of Ultraviolet Air Disinfection. *Am. Rev. Respir. Dis.* **1989**, *140* (6), 1832–1832.

(10) Zaffina, S.; Camisa, V.; Lembo, M.; Vinci, M. R.; Tucci, M. G.; Borra, M.; Napolitano, A.; Cannatà, V. Accidental Exposure to UV Radiation Produced by Germicidal Lamp: Case Report and Risk Assessment. *Photochem. Photobiol.* **2012**, *88* (4), 1001–1004.

(11) *American Conference of Governmental Industrial Hygienists, 2024. Threshold Limit Values and Biological Exposure Indices*.

(12) Ma, B.; Gundy, P. M.; Gerba, C. P.; Sobsey, M. D.; Linden, K. G. UV Inactivation of SARS-CoV-2 across the UVC Spectrum: KrCl* Excimer, Mercury-Vapor, and Light-Emitting-Diode (LED) Sources. *Appl. Environ. Microbiol.* **2021**, *87* (22), e0153221.

(13) Ma, B.; Bright, K.; Ikner, L.; Ley, C.; Seyedi, S.; Gerba, C. P.; Sobsey, M. D.; Piper, P.; Linden, K. G. UV Inactivation of Common Pathogens and Surrogates Under 222 Nm Irradiation from KrCl* Excimer Lamps. *Photochem. Photobiol.* **2023**, *99* (3), 975–982.

(14) Ma, B.; Linden, Y. S.; Gundy, P. M.; Gerba, C. P.; Sobsey, M. D.; Linden, K. G. Inactivation of Coronaviruses and Phage Phi6 from Irradiation across UVC Wavelengths. *Environmental Science & Technology Letters* **2021**. https://doi.org/10.1021/acs.estlett.1c00178.

(15) Robinson, R. T.; Mahfooz, N.; Rosas-Mejia, O.; Liu, Y.; Hull, N. M. UV222 Disinfection of SARS-CoV-2 in Solution. *Sci. Rep.* **2022**, *12* (1), 14545.

(16) Welch, D.; Buonanno, M.; Buchan, A. G.; Yang, L.; Atkinson, K. D.; Shuryak, I.; Brenner, D. J. Inactivation Rates for Airborne Human Coronavirus by Low Doses of 222 Nm Far-UVC Radiation. *Viruses* **2022**, *14* (4). https://doi.org/10.3390/v14040684.

(17) Buchan, A. G.; Yang, L.; Welch, D.; Brenner, D. J.; Atkinson, K. D. Improved Estimates of 222 Nm Far-UVC Susceptibility for Aerosolized Human Coronavirus via a Validated High-Fidelity Coupled Radiation-CFD Code. *Sci. Rep.* **2021**, *11* (1), 19930.

(18) Buonanno, M.; Welch, D.; Shuryak, I.; Brenner, D. J. Far-UVC Light (222 Nm) Efficiently and Safely Inactivates Airborne Human Coronaviruses. *Sci. Rep.* **2020**, *10* (1), 10285.

(19) Schuit, M. A.; Larason, T. C.; Krause, M. L.; Green, B. M.; Holland, B. P.; Wood, S. P.; Grantham, S.; Zong, Y.; Zarobila, C. J.; Freeburger, D. L.; Miller, D. M.; Bohannon, J. K.; Ratnesar-Shumate, S. A.; Blatchley, E. R.; Li, X.; Dabisch, P. A.; Miller, C. C. SARS-CoV-2 Inactivation by Ultraviolet Radiation and Visible Light Is Dependent on Wavelength and Sample Matrix. *J. Photochem. Photobiol. B* **2022**, *233* (January), 112503.

(20) Fujimoto, N.; Nagaoka, K.; Tatsuno, I.; Oishi, H.; Tomita, M.; Hasegawa, T.; Tanaka, Y.; Matsumoto, T. Wavelength Dependence of Ultraviolet Light Inactivation for SARS-CoV-2 Omicron Variants. *Sci.*

Rep. **2023**, *13* (1), 9706.
(21) Link, M. F.; Shore, A.; Hamadani, B. H.; Poppendieck, D. Ozone Generation from a Germicidal Ultraviolet Lamp with Peak Emission at 222 Nm. *Environmental Science & Technology Letters* **2023**. https://doi.org/10.1021/acs.estlett.3c00318.
(22) Peng, Z.; Day, D. A.; Symonds, G. A.; Jenks, O. J.; Stark, H.; Handschy, A. V.; de Gouw, J. A.; Jimenez, J. L. Significant Production of Ozone from Germicidal UV Lights at 222 Nm. *Environmental Science & Technology Letters* **2023**, *10* (8), 668–674.
(23) Peng, Z.; Miller, S. L.; Jimenez, J. L. Model Evaluation of Secondary Chemistry due to Disinfection of Indoor Air with Germicidal Ultraviolet Lamps. *Environmental Science & Technology Letters* **2023**, *10* (1), 6–13.
(24) Barber, V. P.; Goss, M. B.; Franco Deloya, L. J.; LeMar, L. N.; Li, Y.; Helstrom, E.; Canagaratna, M.; Keutsch, F. N.; Kroll, J. H. Indoor Air Quality Implications of Germicidal 222 Nm Light. *Environ. Sci. Technol.* **2023**. https://doi.org/10.1021/acs.est.3c05680.
(25) Graeffe, F.; Luo, Y.; Guo, Y.; Ehn, M. Unwanted Indoor Air Quality Effects from Using Ultraviolet C Lamps for Disinfection. *Environ. Sci. Technol. Lett.* **2023**, *10* (2), 172–178.
(26) Liang, Z.; Zhou, L.; Chen, K.; Lin, Y.-H.; Lai, A. C. K.; Lee, P. K. H.; Sit, P. H. L.; Yin, R.; Chan, C. K. Formation of Secondary Aerosol by 222 Nm Far-UVC Irradiation on SO2. *Atmos. Environ.* **2024**, *330* (120559), 120559.
(27) Burkholder, J. B.; Sander, S. P.; Abbatt, J. P. D.; Barker, J. R.; Cappa, C.; Crounse, J. D.; Dibble, T. S.; Huie, R. E.; Kolb, C. E.; Kurylo, M. J.; Others. *Chemical Kinetics and Photochemical Data for Use in Atmospheric Studies; Evaluation Number 19*; Pasadena, CA: Jet Propulsion Laboratory, National Aeronautics and Space …, 2020. https://trs.jpl.nasa.gov/handle/2014/49199.
(28) Jenks, O. J.; Peng, Z.; Schueneman, M. K.; Rutherford, M.; Handschy, A. V.; Day, D. A.; Jimenez, J. L.; de Gouw, J. A. Effects of 222 Nm Germicidal Ultraviolet Light on Aerosol and VOC Formation from Limonene. *ACS EST Air* **2024**, *1* (7), 725–733.
(29) Peng, Z.; Jimenez, J. L. Radical Chemistry in Oxidation Flow Reactors for Atmospheric Chemistry Research. *Chem. Soc. Rev.* **2020**, *49* (9), 2570–2616.
(30) Dewald, P.; Lelieveld, J.; Crowley, J. NO_3 Reactivity Measurements in an Indoor Environment: A Pilot Study. *Environ. Sci. Atmos.* **2023**, *3* (12), 1778–1790.
(31) Schraufnagel, D. E. The Health Effects of Ultrafine Particles. *Exp. Mol. Med.* **2020**, *52* (3), 311–317.
(32) Turner, M. C.; Jerrett, M.; Pope, C. A.; Krewski, D.; Gapstur, S. M.; Diver, W. R.; Beckerman, B. S.; Marshall, J. D.; Su, J.; Crouse, D. L.; Burnett, R. T. Long-Term Ozone Exposure and Mortality in a Large Prospective Study. *Am. J. Respir. Crit. Care Med.* **2016**, *193* (10), 1134–1142.
(33) Weichenthal, S.; Pinault, L.; Christidis, T.; Burnett, R. T.; Brook, J. R.; Chu, Y.; Crouse, D. L.; Erickson, A. C.; Hystad, P.; Li, C.; Martin, R. V.; Meng, J.; Pappin, A. J.; Tjepkema, M.; van Donkelaar, A.; Weagle, C. L.; Brauer, M. How Low Can You Go? Air Pollution Affects Mortality at Very Low Levels. *Science Advances* **2022**, *8* (39), abo3381.
(34) Kim, K.-H.; Jahan, S. A.; Lee, J.-T. Exposure to Formaldehyde and Its Potential Human Health Hazards. *J. Environ. Sci. Health C Environ. Carcinog. Ecotoxicol. Rev.* **2011**, *29* (4), 277–299.
(35) Keller-Rudek, H.; Moortgat, G. K.; Sander, R.; Sörensen, R. The MPI-Mainz UV/VIS Spectral Atlas of Gaseous Molecules of Atmospheric Interest. *Earth Syst. Sci. Data* **2013**, *5* (2), 365–373.
(36) Stockwell, W. R.; Kirchner, F.; Kuhn, M.; Seefeld, S. A New Mechanism for Regional Atmospheric Chemistry Modeling. *J. Geophys. Res.* **1997**, *102* (D22), 25847–25879.
(37) Peng, Z.; Jimenez, J. L. KinSim: A Research-Grade, User-Friendly, Visual Kinetics Simulator for Chemical-Kinetics and Environmental-Chemistry Teaching. *J. Chem. Educ.* **2019**, *96* (4), 806–811.
(38) Logue, J. M.; McKone, T. E.; Sherman, M. H.; Singer, B. C. Hazard Assessment of Chemical Air Contaminants Measured in Residences. *Indoor Air* **2011**, *21* (2), 92–109.
(39) Nazaroff, W. W. Residential Air-change Rates: A Critical Review. *Indoor Air* **2021**, *31* (2), 282–313.
(40) Krechmer, J. E.; Day, D. A.; Jimenez, J. L. Always Lost but Never Forgotten: Gas-Phase Wall Losses Are Important in All Teflon Environmental Chambers. *Environ. Sci. Technol.* **2020**, *54* (20), 12890–12897.
(41) K. Lai, A. C.; Nazaroff, W. W. MODELING INDOOR PARTICLE DEPOSITION FROM TURBULENT FLOW ONTO SMOOTH SURFACES. *J. Aerosol Sci.* **2000**, *31* (4), 463–476.
(42) Algrim, L. B.; Pagonis, D.; de Gouw, J. A.; Jimenez, J. L.; Ziemann, P. J. Measurements and Modeling of Absorptive Partitioning of Volatile Organic Compounds to Painted Surfaces. *Indoor Air* **2020**. https://doi.org/10.1111/ina.12654.

(43) Donahue, N. M.; Robinson, A. L.; Stanier, C. O.; Pandis, S. N. Coupled Partitioning, Dilution, and Chemical Aging of Semivolatile Organics. *Environ. Sci. Technol.* **2006**, *40* (8), 2635–2643.
(44) Persily, A.; de Jonge, L. Carbon Dioxide Generation Rates for Building Occupants. *Indoor Air* **2017**, *27* (5), 868–879.
(45) Li, M.; Weschler, C. J.; Beko, G.; Wargocki, P.; Lucic, G.; Williams, J. Human Ammonia Emission Rates under Various Indoor Environmental Conditions. *Environ. Sci. Technol.* **2020**. https://doi.org/10.1021/acs.est.0c00094.
(46) Wang, N.; Zannoni, N.; Ernle, L.; Bekö, G.; Wargocki, P.; Li, M.; Weschler, C. J.; Williams, J. Total OH Reactivity of Emissions from Humans: In Situ Measurement and Budget Analysis. *Environ. Sci. Technol.* **2020**. https://doi.org/10.1021/acs.est.0c04206.
(47) Zannoni, N.; Li, M.; Wang, N.; Ernle, L.; Bekö, G.; Wargocki, P.; Langer, S.; Weschler, C. J.; Morrison, G.; Williams, J. Effect of Ozone, Clothing, Temperature, and Humidity on the Total OH Reactivity Emitted from Humans. *Environ. Sci. Technol.* **2021**. https://doi.org/10.1021/acs.est.1c01831.
(48) Wang, N.; Ernle, L.; Bekö, G.; Wargocki, P.; Williams, J. Emission Rates of Volatile Organic Compounds from Humans. *Environ. Sci. Technol.* **2022**, *56* (8), 4838–4848.
(49) Salvador, C. M.; Bekö, G.; Weschler, C. J.; Morrison, G.; Le Breton, M.; Hallquist, M.; Ekberg, L.; Langer, S. Indoor Ozone/human Chemistry and Ventilation Strategies. *Indoor Air* **2019**, *29* (6), 913–925.
(50) Qu, Y.; Zou, Z.; Weschler, C. J.; Liu, Y.; Yang, X. Quantifying Ozone-Dependent Emissions of Volatile Organic Compounds from the Human Body. *Environ. Sci. Technol.* **2023**. https://doi.org/10.1021/acs.est.3c02340.
(51) Peng, Z.; Lee-Taylor, J.; Stark, H.; Orlando, J. J.; Aumont, B.; Jimenez, J. L. Evolution of OH Reactivity in NO-Free Volatile Organic Compound Photooxidation Investigated by the Fully Explicit GECKO-A Model. *Atmos. Chem. Phys.* **2021**, *21* (19), 14649–14669.
(52) Lu, Y. H.; Wang, R. X.; Liu, H. L.; Lai, A. C. K. Evaluating the Performance of UV Disinfection across the 222-365 Nm Spectrum against Aerosolized Bacteria and Viruses. *Environ. Sci. Technol.* **2024**. https://doi.org/10.1021/acs.est.3c08675.
(53) Xiang, J.; Weschler, C. J.; Zhang, J.; Zhang, L.; Sun, Z.; Duan, X.; Zhang, Y. Ozone in Urban China: Impact on Mortalities and Approaches for Establishing Indoor Guideline Concentrations. *Indoor Air* **2019**, *29* (4), ina.12565.
(54) Klepeis, N. E.; Nelson, W. C.; Ott, W. R.; Robinson, J. P.; Tsang, A. M.; Switzer, P.; Behar, J. V.; Hern, S. C.; Engelmann, W. H. The National Human Activity Pattern Survey (NHAPS): A Resource for Assessing Exposure to Environmental Pollutants. *J. Expo. Anal. Environ. Epidemiol.* **2001**, *11* (3), 231–252.
(55) EPA. Chapter 6—Inhalation Rates. In *Exposure Factors Handbook*; U.S. Environmental Protection Agency, 2011.
(56) Chen, C.; Zhao, B. Review of Relationship between Indoor and Outdoor Particles: I/O Ratio, Infiltration Factor and Penetration Factor. *Atmos. Environ. (1994)* **2011**, *45* (2), 275–288.
(57) Nazaroff, W. W.; Weschler, C. J. Indoor Ozone: Concentrations and Influencing Factors. *Indoor Air* **2022**, *32* (1), e12942.
(58) *ASHRAE 62.1-2022*. https://www.techstreet.com/ashrae/standards/ashrae-62-1-2022?product_id=2501063 (accessed 2025-01-13).
(59) Furlow, B. US CDC Announces Indoor Air Guidance for COVID-19 after 3 Years. *Lancet Respir Med* **2023**, *11* (7), 587.
(60) Whalen, J. J. *Environmental Control for Tuberculosis; Basic Upper-Room Ultraviolet Germicidal Irradiation Guidelines for Healthcare Settings Guide*; National Institute for Occupational Safety and Health, Division of Applied Research and Technology, 2009. https://stacks.cdc.gov/view/cdc/5306.
(61) Who. *Roadmap to Improve and Ensure Good Indoor Ventilation in the Context of COVID-19*; 2021; p 38.
(62) Weschler, C. J.; Nazaroff, W. W. Ozone Loss: A Surrogate for the Indoor Concentration of Ozone-Derived Products. *Environ. Sci. Technol.* **2023**, *57* (36), 13569–13578.
(63) He, L.; Hao, Z.; Weschler, C. J.; Li, F.; Zhang, Y.; Zhang, J. J. Indoor Ozone Reaction Products: Contributors to the Respiratory Health Effects Associated with Low-Level Outdoor Ozone. *Atmos. Environ. (1994)* **2025**, *340* (120920), 120920.
(64) Kowalski, W. *Ultraviolet Germicidal Irradiation Handbook*; Springer Berlin Heidelberg: Berlin,

Heidelberg, 2009; pp 1–23.
(65) Ruetalo, N.; Berger, S.; Niessner, J.; Schindler, M. Inactivation of Aerosolized SARS-CoV-2 by 254 Nm UV-C Irradiation. *Indoor Air* **2022**, *32* (9), e13115.
(66) Lu, Y. H.; Shi, X. R.; Li, W. S.; Lai, A. C. K. Wavelength-Specific Inactivation Mechanisms and Efficacies of Germicidal UVC for Airborne Human Coronavirus. *J. Hazard. Mater.* **2024**, *484*, 136666.
(67) Hill, S. C.; Doughty, D. C.; Mackowski, D. W.; Rastogi, V.; Eversole, J. D.; McGrady, D.; Handler, F.; Kesavan, J. Enhanced Survival Fractions of UV-Irradiated Spores in Clusters on a Surface in Air: Measured and Mathematically Modeled Results at 254-Nm. *Aerosol Sci. Technol.* **2023**, 1–21.
(68) Johnston, H. S.; Paige, M.; Yao, F. Oxygen Absorption Cross Sections in the Herzberg Continuum and between 206 and 327 K. *J. Geophys. Res.* **1984**, *89* (D7), 11661–11665.
(69) Kaufman, F. Air Afterglow and Kinetics of Some Reactions of Atomic Oxygen. *J. Chem. Phys.* **1958**, *28* (2), 352–353.
(70) CDC. *COVID data tracker*. Centers for Disease Control and Prevention. https://covid.cdc.gov/covid-data-tracker/ (accessed 2024-02-18).
(71) US Census Bureau. Births Now Outpacing Deaths in over Half the States. **2023**.
(72) Villeneuve, P. J.; Jerrett, M.; Su, J.; Burnett, R. T.; Chen, H.; Brook, J.; Wheeler, A. J.; Cakmak, S.; Goldberg, M. S. A Cohort Study of Intra-Urban Variations in Volatile Organic Compounds and Mortality, Toronto, Canada. *Environ. Pollut.* **2013**, *183*, 30–39.